Search for Dinucleon Decay into Kaons in Super-Kamiokande

M. Litos,[1,†] K. Abe,[2] Y. Hayato,[2,3] T. Iida,[2] M. Ikeda,[2] K. Iyogi,[2] J. Kameda,[2] K. Kobayashi,[2] Y. Koshio,[2] Y. Kozuma,[2] M. Miura,[2] S. Moriyama,[2,3] M. Nakahata,[2,3] S. Nakayama,[2] Y. Obayashi,[2] H. Ogawa,[2] H. Sekiya,[2] M. Shiozawa,[2,3] Y. Suzuki,[2,3] A. Takeda,[2] Y. Takenaga,[2] Y. Takeuchi,[2,3] K. Ueno,[2] K. Ueshima,[2] H. Watanabe,[2] S. Yamada,[2] T. Yokozawa,[2] S. Hazama,[4] C. Ishihara,[4] H. Kaji,[4] T. Kajita,[4,3] K. Kaneyuki,[4,3,*] T. McLachlan,[4] K. Okumura,[4] Y. Shimizu,[4] N. Tanimoto,[4] M. R. Vagins,[3,5] E. Kearns,[1,3] J. L. Stone,[1,3] L. R. Sulak,[1] F. Dufour,[1] J. L. Raaf,[1] B. Henning,[1] M. Goldhaber,[6] K. Bays,[5] D. Casper,[5] J. P. Cravens,[5] W. R. Kropp,[5] S. Mine,[5] C. Regis,[5] M. B. Smy,[5,3] H. W. Sobel,[5,3] K. S. Ganezer,[7] J. Hill,[7] W. E. Keig,[7] J. S. Jang,[8] J. Y. Kim,[8] I. T. Lim,[8] J. B. Albert,[9] T. Wongjirad,[9] R. Wendell,[9] K. Scholberg,[9,3] C. W. Walter,[9,3] S. Tasaka,[10] J. G. Learned,[11] S. Matsuno,[11] Y. Watanabe,[12] T. Hasegawa,[13] T. Ishida,[13] T. Ishii,[13] T. Kobayashi,[13] T. Nakadaira,[13] K. Nakamura,[13,3] K. Nishikawa,[13] H. Nishino,[13] Y. Oyama,[13] K. Sakashita,[13] T. Sekiguchi,[13] T. Tsukamoto,[13] A. T. Suzuki,[14] A. Minamino,[15] T. Nakaya,[15,3] Y. Fukuda,[16] Y. Itow,[17] G. Mitsuka,[17] T. Tanaka,[17] C. K. Jung,[18] G. Lopez,[18] C. McGrew,[18] R. Terri,[18] C. Yanagisawa,[18] N. Tamura,[19] H. Ishino,[20] A. Kibayashi,[20] S. Mino,[20] T. Mori,[20] M. Sakuda,[20] H. Toyota,[20] Y. Kuno,[21] M. Yoshida,[21] S. B. Kim,[22] B. S. Yang,[22] T. Ishizuka,[23] H. Okazawa,[24] Y. Choi,[25] K. Nishijima,[26] Y. Yokosawa,[26] M. Koshiba,[27] M. Yokoyama,[27] Y. Totsuka,[27,*] S. Chen,[28] Y. Heng,[28] Z. Yang,[28] H. Zhang,[28] D. Kielczewska,[29] P. Mijakowski,[29] K. Connolly,[30] M. Dziomba,[30] E. Thrane,[30] and R. J. Wilkes[30]

(The Super-Kamiokande Collaboration)

[1]*Department of Physics, Boston University, Boston, Massachusetts 02215, USA*
[2]*Kamioka Observatory, Institute for Cosmic Ray Research, University of Tokyo, Kamioka, Gifu 506-1205, Japan*
[3]*Institute for the Physics and Mathematics of the Universe (WPI), University of Tokyo, Kashiwa, Chiba 277-8583, Japan*
[4]*Research Center for Cosmic Neutrinos, Institute for Cosmic Ray Research, University of Tokyo, Kashiwa, Chiba 277-8582, Japan*
[5]*Department of Physics and Astronomy, University of California, Irvine, Irvine, California 92697-4575, USA*
[6]*Physics Department, Brookhaven National Laboratory, Upton, New York 11973, USA*
[7]*Department of Physics, California State University, Dominguez Hills, Carson, California 90747, USA*
[8]*Department of Physics, Chonnam National University, Kwangju 500-757, Korea*
[9]*Department of Physics, Duke University, Durham, North Carolina 27708, USA*
[10]*Department of Physics, Gifu University, Gifu, Gifu 501-1193, Japan*
[11]*Department of Physics and Astronomy, University of Hawaii, Honolulu, Hawaii 96822, USA*
[12]*Physics Division, Department of Engineering, Kanagawa University, Kanagawa, Yokohama 221-8686, Japan*
[13]*High Energy Accelerator Research Organization (KEK), Tsukuba, Ibaraki 305-0801, Japan*
[14]*Department of Physics, Kobe University, Kobe, Hyogo 657-8501, Japan*
[15]*Department of Physics, Kyoto University, Kyoto, Kyoto 606-8502, Japan*
[16]*Department of Physics, Miyagi University of Education, Sendai, Miyagi 980-0845, Japan*
[17]*Solar Terrestrial Environment Laboratory, Nagoya University, Nagoya, Aichi 464-8602, Japan*
[18]*Department of Physics and Astronomy, State University of New York, Stony Brook, New York 11794-3800, USA*
[19]*Department of Physics, Niigata University, Niigata, Niigata 950-2181, Japan*
[20]*Department of Physics, Okayama University, Okayama, Okayama 700-8530, Japan*
[21]*Department of Physics, Osaka University, Toyonaka, Osaka 560-0043, Japan*
[22]*Department of Physics, Seoul National University, Seoul 151-742, Korea*
[23]*Department of Systems Engineering, Shizuoka University, Hamamatsu, Shizuoka 432-8561, Japan*
[24]*Department of Informatics in Social Welfare, Shizuoka University of Welfare, Yaizu, Shizuoka 425-8611, Japan*
[25]*Department of Physics, Sungkyunkwan University, Suwon 440-746, Korea*
[26]*Department of Physics, Tokai University, Hiratsuka, Kanagawa 259-1292, Japan*
[27]*The University of Tokyo, Bunkyo, Tokyo 113-0033, Japan*
[28]*Department of Engineering Physics, Tsinghua University, Beijing 100084, China*
[29]*Institute of Experimental Physics, Warsaw University, 00-681 Warsaw, Poland*
[30]*Department of Physics, University of Washington, Seattle, Washington 98195-1560, USA*
(Received 10 October 2013; published 4 April 2014)

A search for the dinucleon decay $pp \to K^+ K^+$ has been performed using 91.6 kton · yr data from Super-Kamiokande-I. This decay provides a sensitive probe of the R-parity-violating parameter λ_{112}''. A boosted decision tree analysis found no signal candidates in the data. The expected background was 0.28 ± 0.19 atmospheric neutrino induced events and the estimated signal detection efficiency

was $12.6\% \pm 3.2\%$. A lower limit of 1.7×10^{32} years has been placed on the partial lifetime of the decay $^{16}O \rightarrow ^{14}CK^+K^+$ at 90% C.L. A corresponding upper limit of 7.8×10^{-9} has been placed on the parameter λ_{112}''.

Dinucleon decay is the name given to the process where the quarks of two bound nucleons interact to produce a decay. This process could be mediated by the exchange of a non–standard model particle. An exclusively mesonic final state would conserve charge, momentum, and angular momentum, and violate only baryon number by two units. In this regard, dinucleon decay is sensitive to different processes than single nucleon decay, which must violate both baryon and lepton number.

In this Letter, we describe our search for dinucleon decay via the reaction $pp \rightarrow K^+K^+$ in $^{16}O \rightarrow ^{14}C$ K^+K^+. Dinucleon decay modes with final-state kaons are particularly interesting in the context of supersymmetry, in which the diagram for the reaction includes R-parity-violating interaction vertices, characterized by the $\Delta B = 1$ coupling constant λ_{112}'' (see Fig. 1). It is expected that dinucleon decay into kaons is the most sensitive experimental probe of the magnitude of λ_{112}'' [1–3]. Several comprehensive reviews of current phenomenological limits on the λ_{ijk}'' parameters exist in the literature [4–6]. Dinucleon decay to kaons also constrains generic [nonsupersymmetric (SUSY)] models of baryon number violation [7].

The Fréjus tracking iron calorimeter experiment [8] is the only other experiment to have performed a direct search for $\Delta B = 2$ dinucleon decay modes with visible final-state particles. The Fréjus Collaboration searched for final states composed of either leptons or pions through such channels as $pp \rightarrow e^+e^+$ and $pp \rightarrow \pi^+\pi^+$ using the iron in the detector as the progenitor nucleus [9]. No evidence was seen for pionic or leptonic decay modes. The Fréjus dinucleon decay study was based on a 2.0 kton·yr exposure, corresponding to about 2.1×10^{31} iron·yrs. Partial lifetime limits were placed on the pionic and leptonic decay modes that were on the order of 10^{30} years [9,10]. The Fréjus study did not include any searches for dinucleon decay into final states with kaons.
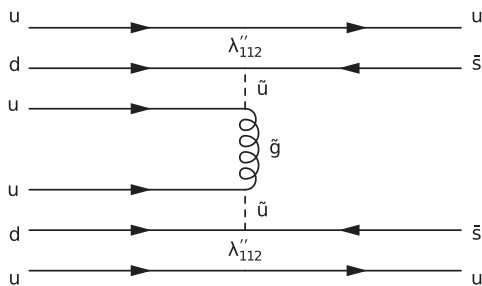
In this Letter, the data collected during the SK-I data-taking period (May 1996–July 2001; 1489.2 days of live time) are analyzed, corresponding to 91.6 kton·yrs or 3.1×10^{33} oxygen·yrs of exposure. The Super-Kamiokande (SK) water Cherenkov detector is located beneath a 2700-m water equivalent overburden of rock, under the peak of Mt. Ikenoyama in Kamioka, Gifu prefecture in Japan. For details on the detector design, calibration, data reduction, and simulations, see Ref. [11]. This study concentrates only on events in which all of the Cherenkov light was fully contained in the inner detector. The data used in this study is the same set used for other proton decay and atmospheric neutrino studies performed at Super-Kamiokande.

There are three dinucleon decay modes with a final state composed exclusively of kaons: $pp \rightarrow K^+K^+$, $pn \rightarrow K^+K^0$, and $nn \rightarrow K^0K^0$. The decay mode into two charged kaons features the most distinct experimental signature. The charged kaons are ejected from the parent nucleus with a momentum of roughly 800 MeV/c, above their Cherenkov threshold in water of 563 MeV/c, and are therefore directly detectable. The muons produced in the kaon decay chain are also above the Cherenkov threshold and are detectable, as are the electromagnetic showers due to gamma-rays from π^0 decay. Decays involving neutral kaons are less efficiently identified, due to the K^0_L escaping the detector and the high branching fraction of K^0_S to $\pi^+\pi^-$, which proves to be a difficult signature to discern in a water Cherenkov detector.

The branching ratios of the three most probable final states of $pp \rightarrow K^+K^+$ are shown in Table I. The third column in the table shows the final-state combinatorics, and the fourth column shows the detectable relative rates as obtained from the Monte Carlo simulation. The detectable relative rates include detection inefficiencies due to hadronic interactions that consume one or both of the K^+ before they are able to decay. The leading hadronic effects

FIG. 1. Feynman diagram for $pp \rightarrow K^+K^+$ in a supersymmetric framework. λ_{112}'' appears in two interaction vertices.

TABLE I. Final-state branching ratios (B.R.) and detectable relative rate (D.R.R.) from the $pp \rightarrow K^+K^+$ Monte Carlo simulation. Only kaon decay branches to $\mu^+\nu_\mu$ and $\pi^+\pi^0$ were considered.

Decay mode	Final state	B.R	D.R.R.
$pp \rightarrow K^+K^+$	$\mu^+\nu_\mu\mu^+\nu_\mu$	40%	30%
	$\mu^+\nu_\mu\pi^+\pi^0$	26%	19%
	$\pi^+\pi^0\pi^+\pi^0$	4%	3%
Total		70%	52%

of this type are charge-exchange interactions ($K^+ n \rightarrow K^0 p$) which occur while the K^+ travels through the water. Charge exchange occurs at a rate of 9.5% per K^+.

The only source of background in this analysis is from multi-ring events produced by multi-GeV atmospheric neutrino interactions. The Monte Carlo program used to model these events is described in Ref. [12]. The rate of these types of events in the Super-Kamiokande detector is about 2.5 per day. Multiring events are produced when mesons from the hadronic recoil produces visible rings. Rings produced by recoiling protons, while generally rare, are also present in the final background sample [13]. Other mechanisms, such as multiple scattering and hadronic inter-actions of pions, can also contribute to multiple background events.

The experimental signature of this dinucleon decay has features not seen in Super-Kamiokande searches for typical proton decay modes, such as $p \rightarrow e^+ \pi^0$ and $p \rightarrow \nu K^+$ [14,15]. The distinguishing features of the signal events are the visible Cherenkov rings produced by charged kaons above the Cherenkov threshold and the large spatial separation between the vertices of the kaon decay products. A cartoon illustration of the event geometry is shown in Fig. 2. Because of the relatively long lifetime of the charged kaons (12 ns), they are expected to travel a distance of about 1.3 m until slowing to a stop and ultimately decaying. About 27% of the kaons in our simulation decayed in flight.

The operating principle of this analysis is to reconstruct all events in the data according to the hypothesis that they were created by dinucleon decay into kaons with a final state corresponding to one of those listed in Table I. The resulting reconstructed variables describing the event under the dinucleon decay hypothesis are then fed into a boosted decision tree trained on Monte Carlo signal and back-ground events which yields an ultimate discriminatory variable representing how signal-like or background-like each event appears to be. The final cut on the boosted decision tree output is optimized based upon the signifi-cance for finding a single signal event.

The event reconstruction is performed in a two-step process. In the first step, each ring is reconstructed on an
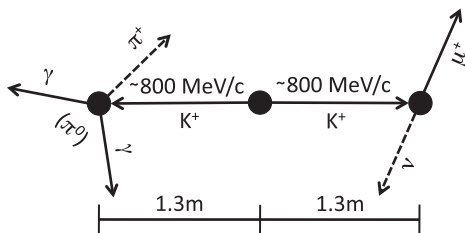

FIG. 2.   Cartoon illustration of an expected event geometry for the final state $pp \rightarrow K^+ K^+ \rightarrow \mu^+ \nu_\mu \pi^+ \pi^0$. The Fermi momentum of the parent nucleons will actually distort the back-to-back symmetry of the kaon vectors. Dashed lines indicate particles undetectable in a water Cherenkov detector.

individual basis using three particle-type hypotheses: K^+, μ^+, and γ. Each ring is assigned a direction of travel, Cherenkov opening angle, and momentum corresponding to all three particle-type hypotheses. Unlike previous SK analyses, where a single event vertex is defined, a newly developed algorithm assigns an independent vertex for each ring. A showering likelihood independent of particle type is also assigned to each ring. The showering likelihood quantifies how likely a ring was to have originated from an electromagnetic showering particle (i.e., $e^\pm$ or γ), or a more massive, nonshowering particle (i.e., p, $K^\pm$, $\pi^\pm$, or $\mu^\pm$) based on the light pattern of the ring [12]. A special light-masking algorithm is utilized in the ring reconstruction that allows a single ring to be considered independently of all other light in the detector [16]. This masking is crucial for resolving the multiple particle vertices in the $pp \rightarrow K^+ K^+$ signal events.

In the second step, all of the rings in the event are considered together, after which the final particle-type assignment for each ring is made. The reconstructed ring variables and the event topology are used in conjunction to classify each ring as either a K^+ candidate, μ^+ candidate, or γ candidate—the three detectable particle types in the signal events—using the $pp \rightarrow K^+ K^+$ hypothesis. We note that the π^+ from $K^+ \rightarrow \pi^+ \pi^0$, though just above the Cherenkov threshold, would not generate enough light to be detectable amidst the many other, brighter rings, and thus no attempt is made to identify them in this study.

After having classified all rings as either K^+, μ^+, or γ candidates, we categorize the event based on the break-down of its constituent rings. Monte Carlo studies show that only certain event categories are likely to arise from a dinucleon decay event by this method of ring accounting. Eight event categories are selected to continue past the event reconstruction and precuts (described below) phase of the analysis, and are listed in the left column of Table II.

Just prior to the selection on event category, the follow-ing precuts are applied to the data and Monte Carlo samples to reduce a significant portion of the background while retaining the majority of the signal: $3 \leq$ number of found rings ≤ 5; $1000 \leq$ total number of photoelectrons in the inner detector $\leq 11\,000$; $0 \leq$ number of found muon-decay electrons ≤ 2; distance from event vertex to nearest wall > 200 cm, where the event vertex is determined by the event's best kaon candidates resulting from the ring reconstruction method described previously. A total of 27 events in the data pass both the precuts and event category selection, with an expected background of 33.9 events and a signal efficiency of 21.9% predicted by the Monte Carlo calculation.

Following precuts and selection on event category, the remaining events are processed by a boosted decision tree (BDT) [17]. One of the primary advantages of a BDT over other multivariate techniques is that the inclusion of weak discriminatory variables does not lessen its performance [18]. In total, 37 BDT input variables are used in this analysis [16].

TABLE II.   Efficiency of all simulated $pp \rightarrow K^+K^+$ events, expected neutrino background events, and actual data events passing the precuts and the final BDT cut for the $pp \rightarrow K^+K^+$ Monte Carlo, the atmospheric neutrino Monte Carlo, and the SK-I data, respectively. Poisson probabilities to observe at least the number of events in the data given the expected background in each category are shown in parentheses, where it is assumed all events in the data were induced by atmospheric neutrinos.

| Category | $pp \rightarrow K^+K^+$ MC efficiency (%) | | Atm. ν MC events/SK-I exposure | | SK-I Data events | |
	Precuts	BDT	Precuts	BDT	Precuts (P_{Poisson})	Final BDT Cut
$K^+K^+\mu^+$	6.1	5.0	0.6	0.07	0 (53%)	0
$K^+\mu^+\mu^+$	5.6	1.8	6.1	0.08	5 (42%)	0
$K^+\mu^+\gamma\gamma$	4.6	1.0	26.1	0.08	22 (25%)	0
$K^+K^+\mu^+\mu^+$	2.7	2.5	0.0	0.00	0 (98%)	0
$K^+K^+\gamma$	1.1	0.8	0.4	0.02	0 (67%)	0
$K^+K^+\mu^+\gamma$	1.1	1.0	0.3	0.03	0 (73%)	0
$K^+K^+\gamma\gamma$	0.6	0.3	0.3	0.00	0 (75%)	0
$K^+K^+\mu^+\gamma\gamma$	0.2	0.2	0.1	0.00	0 (93%)	0
Total	21.9	12.6	33.9	0.28	27 (13%)	0

The most powerfully discriminating BDT input variables are the distance between the reconstructed vertices of the kaon-decay product candidates (e.g., two μ^+ candidate vertices produced in the same event), and the reconstructed momentum of the K^+ candidates, which assumes the candidate particles have a mass of 493.7 MeV/c^2. In the case of the former, the vertex separation distance is large for the signal events, in which the kaon-decay points are spatially separated, and short for the background events, in which all particles originate from a single neutrino interaction vertex. In the case of the latter, the distribution of the K^+ candidate momenta for the signal should be strongly peaked around 800 MeV/c. After precuts and selection on event category, remaining atmospheric neutrino background events have a broader distribution of reconstructed kaon candidate momentum. The BDT input distributions for these variables are shown in Fig. 3 for the Monte Carlo and the SK-I data.

The ROOT-based TMVA [18] package is used to execute the boosted decision tree. The adaptive boosting method is used with 500 trees, and the Gini index is used for the node separation criteria. The cost complexity method is used to prune the BDT after training.

The placement of the final cut on the BDT output is determined by the point which maximizes the significance (Sig./$\sqrt{\text{Sig.} + \text{Bkg.}}$) for identifying one simulated signal event among the number of simulated background events predicted to pass precuts and selection on event category. The background was modeled using the Super-Kamiokande atmospheric neutrino Monte Carlo calculation normalized to the SK-I livetime. By this criteria, the final cut point is determined to be at 0.12, yielding a signal efficiency of 12.6% ± 3.2% and an expected background of 0.28 ± 0.19 events.

The event categories with the highest detection efficiencies in the final signal Monte Carlo sample which passed

the BDT all corresponded to the $K^+K^+ \rightarrow \mu^+\nu_\mu\mu^+\nu_\mu$ final state, shown in Table II. The purities of the ring classifications for the final signal sample are 93%, 82%, and 67% for the K^+, μ^+, and γ candidates, respectively. In about
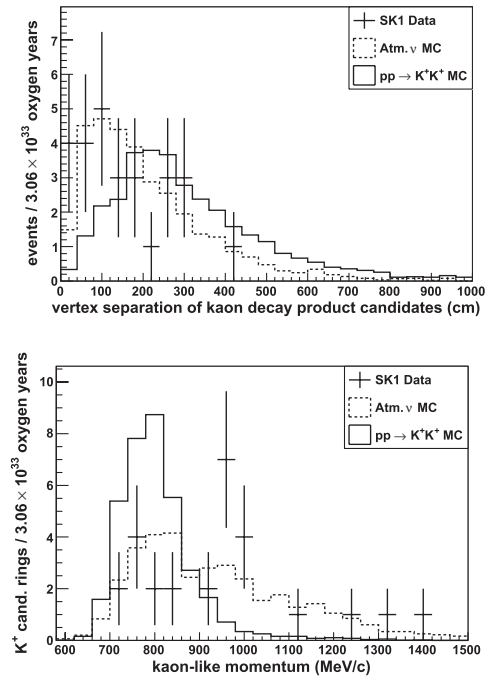

FIG. 3.   Two highly discriminating variables used as inputs for the BDT. Top: Reconstructed vertex separation of kaon-decay product candidates (e.g., two μ^+ candidates). Plots are generated after precuts. Bottom: Reconstructed momentum of K^+ candidates, which assumes the candidate particles have a mass of 493.7 MeV/c^2. Plots are generated after precuts and selection on event category. The number of entries per event in a histogram depend on the BDT event category. The integral of the $pp \rightarrow K^+K^+$ Monte Carlo is normalized to the atmospheric neutrino Monte Carlo.

two-thirds of the final signal sample every ring in the event is correctly classified.

The background Monte Carlo sample remaining after the final BDT cut is dominated by charged-current ν_μ interactions in which one or more pions are produced. About half of the K^+ candidate rings in the simulated background events are generated by muons. The remaining half are mostly generated by charged pions and protons. None of the rings in the final background sample are generated by kaons. About half of the μ^+ candidates are generated by charged pions; the other half are generated by muons, protons, electrons, and gammas in roughly equal amounts. Two-thirds of the γ candidates are generated by gammas; the remaining third is generated by electrons. The strength of the showering or nonshowering likelihood in determining the particle type is clearly demonstrated here.

The primary source of systematic error for the signal detection efficiency arises from the uncertainty in the Fermi momentum of the parent nucleons, which is estimated to be $\pm 24\%$ of the Fermi momentum values used in simulations of the signal. The Fermi motion in our simulation is based on the model used by Nakamura *et al.* [19], and the estimated error is based on the difference between their experimental data and the prediction of the model. The Fermi momentum determines the opening angle between the two kaons, which has a strong influence on ring classification and signal-to-background discrimination. The total systematic error on the signal efficiency is estimated to be 25% [16].

The largest source of systematic error for the background estimation (50%) arose from uncertainties related to the simulation of pion propagation through water. The second largest source of systematic uncertainty (30%) is from training bias of the BDT method. This was estimated by comparing a Monte Carlo set that was independent of the training set used to construct the BDT. The third largest source (20%) is related to hadronic effects of pions propagating through the nucleus in the atmospheric neutrino background. The total systematic error on the background rate is estimated to be 68% [16].

The final boosted decision tree output for the data is overlaid on the signal and background Monte Carlo in Fig. 4. A breakdown of the signal efficiency, expected background, and events in the data after the precuts stage (including selection on event category) and after the BDT stage is shown in Table II. No signal candidate events are found in the data. A partial lifetime limit for the dinucleon decay channel $pp \rightarrow K^+ K^+$ is calculated per oxygen nucleus at a 90% confidence level, giving

$$\tau / BR_{pp \rightarrow K^+ K^+} > 1.7 \times 10^{32} \text{years}.$$

This limit is about 2 orders of magnitude larger than the previously published limits for dinucleon decay modes established by Fréjus [10].
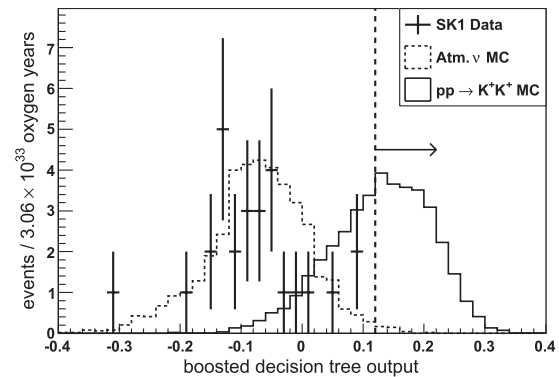

FIG. 4. Final output of the decision tree. Events to the right of the cut at 0.12 are considered signal candidates. All data points are consistent with background; no signal candidates are found in the data. Final signal efficiency: $12.6\% \pm 3.2\%$. Final expected background contamination: 0.28 ± 0.19 events.

Using our partial lifetime limit for $pp \rightarrow K^+ K^+$, we calculate a corresponding upper limit on the magnitude of the $\Delta B = 1$ R-parity-violating parameter λ_{112}'' following the relation given by Ref. [3], where we have assumed the ratio between the SUSY and hadronic scales to be 1.1×10^{-3} and a common superpartner mass of 300 GeV/c^2. Our upper-limit calculation is

$$|\lambda_{112}''| < \left(\frac{0.64 \text{years}}{\tau_{pp \rightarrow K^+ K^+}}\right)^{1/4} = 7.8 \times 10^{-9}.$$

Our new constraint on λ_{112}'' is over two orders of magnitude more restrictive than $\sim 10^{-6}$, the estimate based on rough nuclear lifetime limits of 10^{30} years [3–6].

*Deceased.
†Present address: SLAC National Accelerator Laboratory, Menlo Park, CA 94025, USA.

[1] A. Barbieri and A. Masiero, Nucl. Phys. **B267**, 679 (1986).
[2] S. Dimopoulos and L. Hall, Phys. Lett. B **196**, 135 (1987).
[3] J. L. Goity and M. Sher, Phys. Lett. B **346**, 69 (1995).
[4] R. Barbier, C. Bérat, M. Besançon, M. Chemtob, A. Deandrea, E. Dudas, P. Fayet, S. Lavignac, G. Moreau, and E. Perez, Phys. Rep. **420**, 1 (2005).
[5] M. Chemtob, Prog. Part. Nucl. Phys. **54**, 71 (2005).
[6] A. Y. Smirnov and F. Vissani, Phys. Lett. B **380**, 317 (1996).
[7] J. M. Arnold, B. Fornal, and M. B. Wise, Phys. Rev. D **87**, 075004 (2013).
[8] C. Berger, A. Hofmann, H. Mönch, F. Raupach, P. Schleper, G. Schmitz, J. Tutas, B. Voigtländer, C. Arpesella, and

Y. Benadjal, Nucl. Instrum. Methods Phys. Res., Sect. A **262**, 463 (1987).

[9] C. Berger, M. Froehlich, H. Moench, R. Nisius, and F. R. ldots, Phys. Lett. B **269**, 227 (1991).

[10] C. Amsler, M. Doser, M. Antonelli, D. M. Asner, K. S. Babu, H. Baer, H. R. Band, R. M. Barnett, E. Bergren, and J. Beringer, Phys. Lett. B **667**, 1 (2008).

[11] S. Fukuda *et al.*, Nucl. Instrum. Methods Phys. Res., Sect. A **501**, 418 (2003).

[12] Y. Ashie, J. Hosaka, K. Ishihara, Y. Itow, J. Kameda, Y. Koshio, A. Minamino, C. Mitsuda, M. Miura, and S. Moriyama, Phys. Rev. D **71**, 112005 (2005).

[13] M. Fechner, K. Abe, Y. Hayato, T. Iida, M. Ikeda, J. Kameda, K. Kobayashi, Y. Koshio, M. Miura, and S. Moriyama, Phys. Rev. D **79**, 112010 (2009).

[14] H. Nishino *et al.*, Phys. Rev. Lett. **102**, 141801 (2009).

[15] K. Kobayashi *et al.*, Phys. Rev. D **72**, 052007 (2005).

[16] M. Litos, Ph.D thesis, Boston University, 2010.

[17] T. Hastie, R. Tibshirani, and J. J. H. Friedman, *The Elements of Statistical Learning* (Springer, New York, 2001), Vol. 1.

[18] A. Hocker, P. Speckmayer, J. Stelzer, F. Tegenfeldt, H. Voss, K. Voss, A. Christov, S. Henrot-Versille, M. Jachowski, and A. Krasznahorkay, Jr, *Proc. Sci.*, ACAT2007 (**2007**) 040.

[19] K. Nakamura, S. Hiramatsu, and T. Kamae, Nucl. Phys. **A268**, 381 (1976).